SAND2020-11528J

Ducted Fuel Injection vs. Conventional Diesel Combustion: Extending the Load Range in an Optical Engine with a Four-Orifice Fuel Injector

Christopher W. Nilsen, Drummond E. Biles, Boni F. Yraguen, Charles J. Mueller
Sandia National Laboratories

Abstract

Ducted fuel injection (DFI) is a technique to attenuate soot formation in compression-ignition engines relative to conventional diesel combustion (CDC). The concept is to inject fuel through a small tube inside the combustion chamber to reduce equivalence ratios in the autoignition zone relative to CDC. DFI has been studied at loads as high as 8.5 bar gross indicated mean effective pressure ($IMEP_g$) and as low as 2.5 bar $IMEP_g$ using a four-orifice fuel injector. Across previous studies, DFI has been shown to attenuate soot emissions, increase NO_x emissions (at constant charge dilution), and slightly decrease fuel-conversion efficiencies for most tested points. This study expands on the previous work by testing 1.1 bar $IMEP_g$ (low-load/idle) conditions and 10 bar $IMEP_g$ (higher-load) conditions with the same four-orifice fuel injector, as well as examining potential causes of the degradations in NO_x emissions and fuel-conversion efficiencies. DFI and CDC are directly compared at each operating point in the study. At the low-load condition, the intake charge dilution was swept to elucidate the soot and NO_x performance of DFI. The low-load range is important because it is the target of impending, more-stringent emissions regulations, and DFI is shown to be a potentially effective approach for helping to meet these regulations. The results also indicate that DFI likely has slightly decreased fuel-conversion efficiencies relative to CDC. The increase in NO_x emissions with DFI is likely due to longer charge-gas residence times at higher temperatures, which arise from shorter combustion durations and advanced combustion phasing relative to CDC.

Introduction

Diesel engines are still an important technology for transporting people and goods around the world. They are used for these applications because of their inherently high fuel-conversion efficiencies, the high energy densities of liquid fuels, and the easy availability of suitable fuels. The main downside to diesel engines is their soot and nitrogen oxides (NO_x) emissions, which are known toxins. Soot is also a climate forcing species, second only to carbon dioxide [1]. Because of the benefits of diesel engines, there is significant interest in developing technologies that could be used to address the emissions downsides [2-5]. These technologies include homogeneous-charge compression-ignition (HCCI), low-temperature gasoline combustion (LTGC), and others [6-12]. However, these alternative technologies are challenging to control across a wide load range, with variation in fuels and ambient conditions. Currently diesel engines use aftertreatment systems to attenuate soot and NO_x emissions [13]. These systems are often complicated, expensive, require regular maintenance, and may increase fuel consumption.

Leaner lifted-flame combustion (LLFC) is a mixing-controlled compression-ignition (MCCI) combustion strategy where the combustion is soot free. LLFC occurs when the equivalence ratio at the lift-off length is less than approximately two [14-16]. Lift-off length is defined as the distance between the fuel injector tip and the location where the autoignition zone stabilizes in MCCI [17,18]. LLFC has been achieved in an engine, but it could not be sustained across a wide range of loads and operating conditions [15,19]. This was due to the shortening of lift-off lengths due to high temperatures and interaction between sprays as more orifices were used. A new approach was needed to expand the operating range of LLFC to higher loads. Ducted fuel injection (DFI) was developed to assist in achieving LLFC.

DFI aims to address the emissions issues of diesel engines without significant penalties in controllability or efficiency by achieving LLFC at higher load levels. DFI was created with the goal of enhancing the entrainment and mixing of charge-gas with fuel. This results in leaner mixtures at the lift-off length, which attenuates the formation of soot. Exhaust-gas recirculation (EGR) is effective at mitigating NO_x emissions, but typically comes at a significant soot emissions penalty, especially at high levels of charge dilution. DFI avoids this penalty by attenuating the soot formation that would have been created with increased charge dilutions, thereby enabling the use of EGR for more-cost-effective NO_x control over a wider range of conditions. A study by Ou et al. states that a 50% attenuation of engine-out NO_x emissions could result in a 50% reduction in total aftertreatment system cost [20].

DFI is a mechanical solution that conceivably could be retrofitted into existing engines. A retrofit could allow older engines to comply with newer emissions standards, enabling the continued use of older equipment without replacing the entire machine or even the entire engine. Currently there are over one billion passenger vehicles on the world's roads. Over 99.7% of these use internal combustion engines (ICEs) [21]. There are additional ICEs in commercial vehicles, ships, locomotives, and off-road equipment. If even a small fraction of these engines were upgraded with DFI, the economic and environmental benefits could be significant.

Ducted fuel injection concept

The DFI concept is inspired by the Bunsen burner. The Bunsen burner is a metal tube which has a gaseous fuel injected down the center of it [22]. There are vents at the base of the Bunsen burner where air can enter the tube. The high velocity of the fuel jet entrains air into the tube and the fuel and air mix while traveling through the tube. Enhanced entrainment and mixing enable low-soot combustion that was not possible with previous burner types.

DFI applies the Bunsen burner concept to conventional diesel combustion (CDC), which allows sufficient fuel/charge-gas mixing before autoignition such that LLFC is sustained. Since soot is mitigated by DFI, EGR can be used to lower engine-out NO_x emissions without inducing a smoke penalty. A schematic of DFI is shown in Figure 1.

DFI was first reduced to practice in a constant-volume combustion vessel [23]. A subsequent literature review by Gehmlich et al. of DFI-like devices suggested that fuel injection down the center of a duct inside an engine could enhance mixing [24], indicating that DFI could help to facilitate the achievement of LLFC inside of an engine. The literature review does not include cases with velocity, temperature, and density gradients as large as those that are likely to be present inside of a DFI-equipped engine.

Previous work has explored the effectiveness of DFI versus free spray (i.e., CDC) in both combustion vessels and ICEs. A variety of duct designs were tested in a constant-volume combustion-vessel in two different studies that influenced the duct designs tested in all following studies [23,24]. Gehmlich et al. also tested the δ duct design that will be used in this study. The δ design features a rounded inside of the inlet and a tapered outside of the outlet of the duct. In their work they also established the duct naming convention that will be used for this study. The naming convention for the ducts is as follows: D(*diameter*)L(*length*)G(*standoff distance*)(*duct geometry*), where D, L, and G are defined as shown in Figure 2 and all values are given in millimeters. The lift-off length is shown as H in Figure 2.

Two aditional studies have been carried out in a constant-pressure combustion-vessel. Fitzgerald et al. compared the results of DFI in the constant-flow combustion-vessel to a numerical model to understand how DFI works [25]. This study found that DFI reduces the entrainment of air into the spray, resulting in cooler mixtures that delay igntion. At the same time, the reduced entrainment maintained higher velocities, and resulted in longer lift-off lengths. The study concluded that these two effects create lower equivalence ratios at the lift-off length and therefore lower soot. The second study by Svensson and Martin investigated the effect of length and standoff distance in a constant-pressure combustion-vessel and found longer ducts and smaller gaps worked best to the limits tested [26].

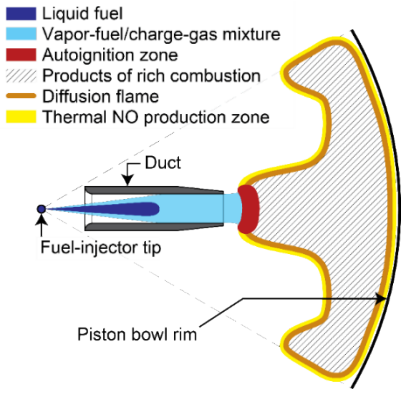

Figure 1. Schematic of ducted fuel injection concept on a single spray.

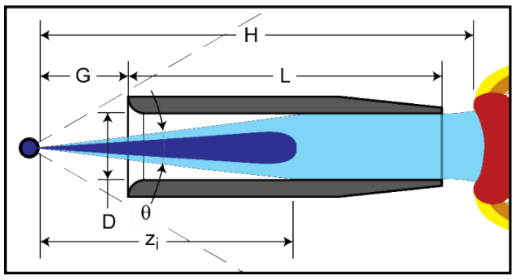

Figure 2. Schematic of important DFI parameters. The duct in this image has the δ geometry.

The first study to look at DFI in an engine was conducted by Nilsen et al. [27]. This study used a two-orifice injector with two ducts in an optical research engine. This study demonstanted that DFI could effectively attenuate soot formation in an engine when compared to CDC. It also showed that DFI could break the soot-NO_x tradeoff with charge dilution. A study by Tanno et al. also studied DFI in an engine [28]. A four-orifice injector with a four-duct configuration was used in a different optical research engine. This study also found that DFI could attenuate soot formation in an engine. Tanno et al. also used numerical modeling to develop an understanding of how DFI works. They found that DFI reduces the peak equivalence ratio at the lift-off length.

Li et al. used Schlieren imaging to look at the characteristics of DFI sprays in a constant-volume combustion-vessel [29]. The study used spray penetration, spray area, and spray angle to develop an understanding of how DFI affects the entrainment of air into the spray. It found that DFI had faster spray penetration and a larger spray angle. The study concluded that DFI has more entrainment than a free spray after the duct.

In a previous study, a four-orifice injector with four ducts was employed in an optical research engine [30]. It expanded on the aforementioned studies by increasing the load of the engine and broadening the range of conditions tested. The parameters swept were charge dilution, start of combustion (SOC) timing, injection pressure, injection duration, intake temperature, and intake pressure. It showed that DFI could maintain the positive soot attenuation effects seen in previous studies at higher loads and across all of the conditions tested.

The present study expands on the previous work of Nilsen et al. by further expanding the load range for DFI. The low-load portion of the study looks at the effect of low injection pressure and a short injection duration, while the higher-load portion includes high injection pressure and a long injection duration. The purpose of this is to understand how the same injector configuration could work across a wide range of loads.

Experimental setup

The optical engine can run a wide range of conditions representative of those in modern turbocharged diesel engines. The engine has optical access through a fused-silica window in the piston bowl. A schematic of the engine is shown in Figure 3. The fuel injector is mounted in the cylinder head, at the center of the cylinder. It is surrounded by the four valves. The engine-out emissions of NO_x, carbon monoxide (CO), carbon dioxide (CO_2), hydrocarbons (HC), and oxygen (O_2) were measured using a set of Califonia Analytical Instruments analyzers. The particulate matter (PM) emissions were

measured using an AVL 415S smoke meter. The in-cylinder pressures were measured using an AVL QC34C transducer.

A common-rail solenoid-actuated injector was used for this study, which was equiped with a four-orifice tip with 110-µm diameter orifices. The low-load portion of the study used 80-MPa injection pressures while the higher-load portion used 240-MPa injection pressures. Injection duration was chosen to achieve the desired load for each of the sweeps. SOC was maintained at top dead center (TDC) for all of the conditions tested. SOC was calculated based on the point where the apparent heat release rate (AHRR) becomes positive. The injection timing was adjusted to maintain a constant SOC. A summary of the test conditions is shown in Table 1. The fuel used was a No. 2 S15 diesel emissions certification fuel, called CF_B. The duct-holder setup used in this study holds four ducts with a 140° included angle and equal rotational separation. Each duct has a D2L12G3δ geometry, a design that showed promising results in previous engine DFI studies [27]. A rendering of the four-duct configuration with the D2L12G3δ ducts installed is shown in Figure 4.

The optical engine also allowed for optical diagnositcs to be used such as spatially integrated natural luminosity (SINL). SINL was important because the engine-out soot levels were too low to measure with standard particulate matter (PM) measurement equipment at some conditions. This engine and its capabilities have been documented elsewhere [15,31].

The engine was run in a skip-fired mode where it was fired once every four cycles. This sequence was chosen to yield sufficiently high exhaust emissions levels to stay above the sensitivity limits of the instruments. There are 180 fired cycles for each engine run, and at least three engine runs were conducted for each condition. The engine was maintained at its temperature set point using an external heater to heat its water-antifreeze coolant mixture. The temperature of the coolant is directly measured and controlled. The temperatures of the ducts, piston, and cylinder walls were not measured. The intake charge-gas temperature was maintained at the same temperature as

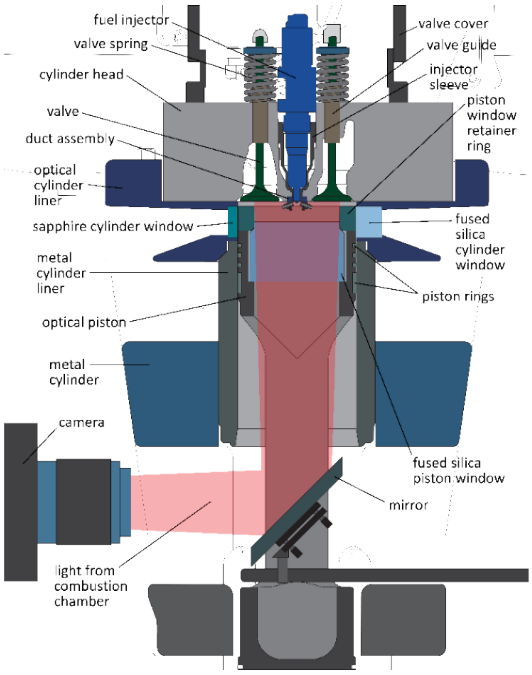

Figure 3. Optical-engine schematic. The camera used in this study is a Photron SA-Z.

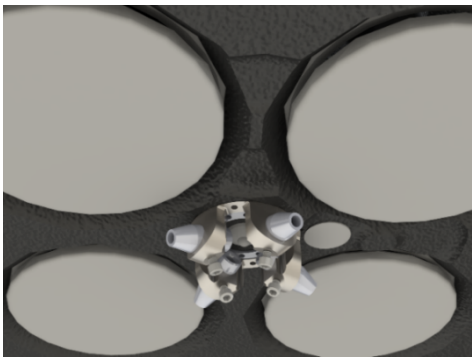

Figure 4. Rendering of 4 duct DFI holder installed in the engine. The ducts shown are D2L12G3δ.

the engine coolant by heating the air prior to its entering the engine. Keeping the engine and intake at the same temperature minimizes the effects of heat transfer in the intake manifold on the results. The specific conditions used in this study are shown in Table 1.

Natural luminonsity (NL) is emitted primarily by hot soot. The NL was measured using a Photron SA-Z high-speed camera with a Nikon 105-mm f/2.8 lens. Images were recorded starting at 5 crank angle degrees (CAD) before the planned SOC and continuing for 50 CAD. The camera recorded at a resolution of 640 × 640 pixels with a frequency of 1 image every 0.5 CAD. The exposure duration and aperture settings were adjusted to prevent the image from saturating while using as much of the dynamic range of the sensor as possible. A 600-nm, short-wave-pass filter and a 3-mm-thick heat-absorption filter (Schott KG3) were used to suppress infrared and red light contributions to the NL signal. SINL is calculated from the NL images by integrating the counts of the pixels located inside the piston-bowl area of the image. ΣSINL is calcuated as a scalar value for each cycle. ΣSINL is the time integral of the time-dependent SINL signal.

Table 1. Experimental test conditions.

	Low Load	Higher Load
Fuel	CF_B	
Speed	1200 RPM	
Displacement	1.72 L	
Duration of injection (DOI, commanded)	1250 µs	4500 µs
Injection pressure	80 MPa	240 MPa
Injector-tip configuration	4 × 0.110 mm × 140°	
Ducts	D2L12G3δ vs. none	
Start of combustion timing (SOC)	0.0 CAD ATDC	
Charge dilution (XO_2)	14, 16, 18 mol% O_2	16 mol% O_2
Global equivalence ratio	0.12, 0.11, 0.093	0.35
Intake manifold absolute pressure (IMAP)	1.5 bar	3.0 bar
Intake manifold temperature (IMT)	90 °C	
Coolant temperature	90 °C	

Charge dilution was swept from 14 to 18 mol% O_2 at approximately 1 bar gross indicated mean effective pressure ($IMEP_g$). $IMEP_g$ is the gross indicated work done by the engine divided by the displacement of the engine. Therefore, it is the integral of pressure versus volume from 180° before TDC to 180° after TDC during the compression and expansion strokes. This load was chosen because it is representative of low-load engine operation. Studying low-load emissions is important because many engines spend a significant amount of time at low-load and idle conditions. For this section, the emissions index (EI) will be used. The EI is given in units of grams emission per kilogram of fuel [g/kg_{fuel}]. Fuel is still burned at low load, so EI emissions do not approach infinity at low-load levels (in contrast to indicated-specific emissions). The fuel-conversion efficiency, η_f, is the ratio of the work done during the combustion process and the energy contained in the fuel injected. An intake manifold absolute pressure (IMAP) of 1.5 bar was chosen to match the in-cylinder pressures at TDC of a modern diesel engine having a 16.5:1 compression ratio at low loads. The optical engine has a geometric compression ratio of 12.5:1. The intake manifold temperature (IMT) of 90 °C was chosen because it matches the in-cylinder temperatures at TDC of a 16.5:1 compression ratio engine with an IMT of 53 °C.

The compression is assumed to be polytropic with an exponent of n_{comp}. Table 2 shows the assumptions for these calculations.

Table 2. Compression ratio compensation table. The 12.5:1 column shows the inputs and the 16.5:1 column shows the outputs.

Compression ratio	12.5:1	16.5:1
n_{comp}	1.39	1.39
Intake temperature	90 °C	53 °C
Intake pressure (low-load)	1.5 bar	1.0 bar
Intake pressure (Higher-Load)	3.0 bar	2.04 bar

The higher-load conditions were chosen to maximize the load that could be achieved in this engine with this injector tip. An injection pressure of 240 MPa is the highest practical injection pressure with the current fuel system configuration, while 4500 µs approaches the maximum realistic duration for a fuel injection event. A 3.0 bar IMAP was chosen because it was the highest IMAP that could be

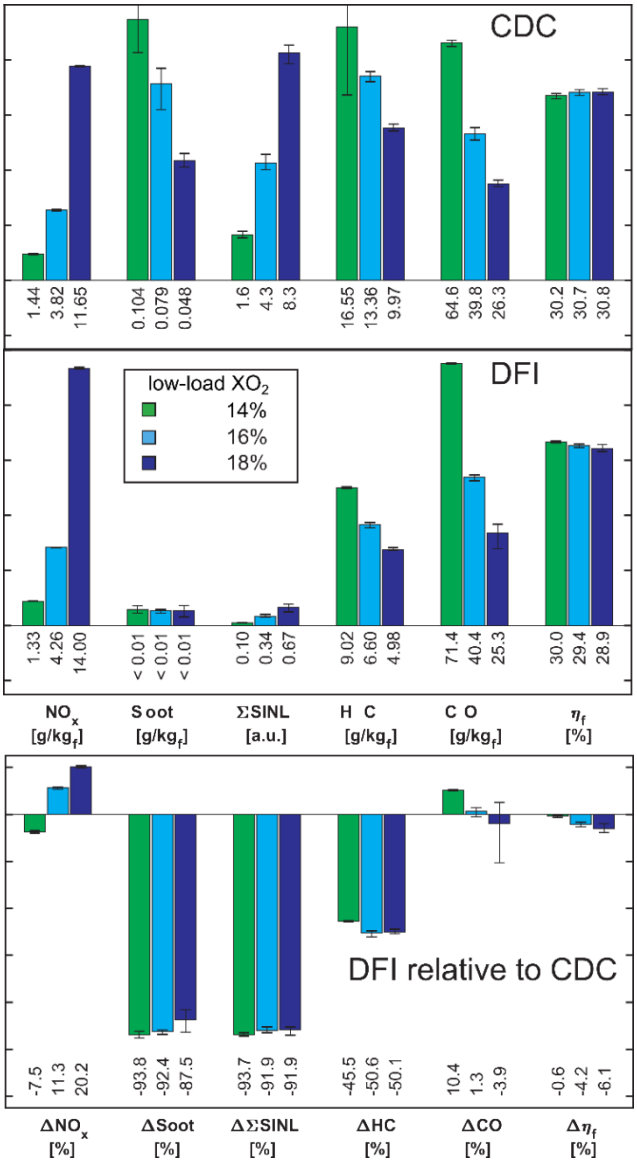

Figure 5: NO_x, soot, ΣSINL, HC, CO, and η_f (fuel-conversion efficiency) for CDC and DFI (upper two plots), and the percent change for DFI relative to CDC (bottom plot) for the low-load charge-dilution sweep.

achieved with the current intake system. This IMAP is equivalent to 2.04 bar in the 16.5:1 compression ratio engine that was mentioned in the preceding paragraph.

Results

Low-Load Charge-Dilution Sweep

Soot attenuation

Figure 5 shows the emissions and efficiency results for CDC and DFI. The percent difference shown is the relative difference for DFI compared to CDC. It is calculated by taking the difference between the CDC and DFI values and then dividing by the CDC value. The percent difference can also be deceptive if an instrument is at its lower sensitivity limit, because it cannot get any lower, while the higher value to which it is being compared can change significantly. The error bars represent the minimum and maximum observed values for the variable over the replicate measurements. The bar itself is the average value for the variable. Percent difference is calculated the same way for the other data in this study; i.e., it is a relative difference rather than an absolute difference. This is true even for fuel-conversion efficiency (η_f).

Figure 5 shows that soot increases significantly for CDC as XO_2 decreases. A similar trend is not observed with DFI because the instrument is at or below its lower sensitivity limit. A further attenuation of soot is expected as XO_2 decreases with DFI, but this study stopped at an XO_2 value of 14 mol%.

Since soot levels are below the detection limit of the smoke meter for DFI, Figure 6 shows examples of NL images from which ΣSINL is calculated. The top-left corner of each image shows the CAD for the image, and the bottom-left corner indicates the corresponding time after commanded start of injection. The top-right corner of the image at the top of each column shows the gain for all the images in that column, and the bottom-right corner shows the cycle number from which the images were taken. The gain is calculated based on the exposure duration and lens aperture used to capture each movie. The DFI images are on the left and CDC is on the right. It can be observed that the soot in the NL images with DFI covers less of the image area than in the CDC images. The brightness in both sets of images appears to be similar, but the camera gain for DFI is approximately 2 times that for CDC.

The ΣSINL decrease with decreasing XO_2 is due at least in part to a reduction in intensity because of lower in-cylinder temperatures. Because of the temperature effect, it is not possible to compare ΣSINL directly across charge dilution levels. However, CDC and DFI can be compared at the same charge dilution. In this regard, DFI is observed to attenuate ΣSINL by between 91% and 94%.

The DFI images in Figure 6 show that DFI produces significantly less NL over the course of the entire combustion event. Moreover, DFI does not produce significant SINL after 10 CAD, whereas CDC produces measurable SINL to 20 CAD ATDC. This indicates that less hot soot is produced and is present later in the combustion process for DFI.

Engine-out NO_x, HC, and CO emissions

Figure 5 shows that both DFI and CDC monotonically attenuate NO_x with decreased XO_2. The percent difference value shows that NO_x

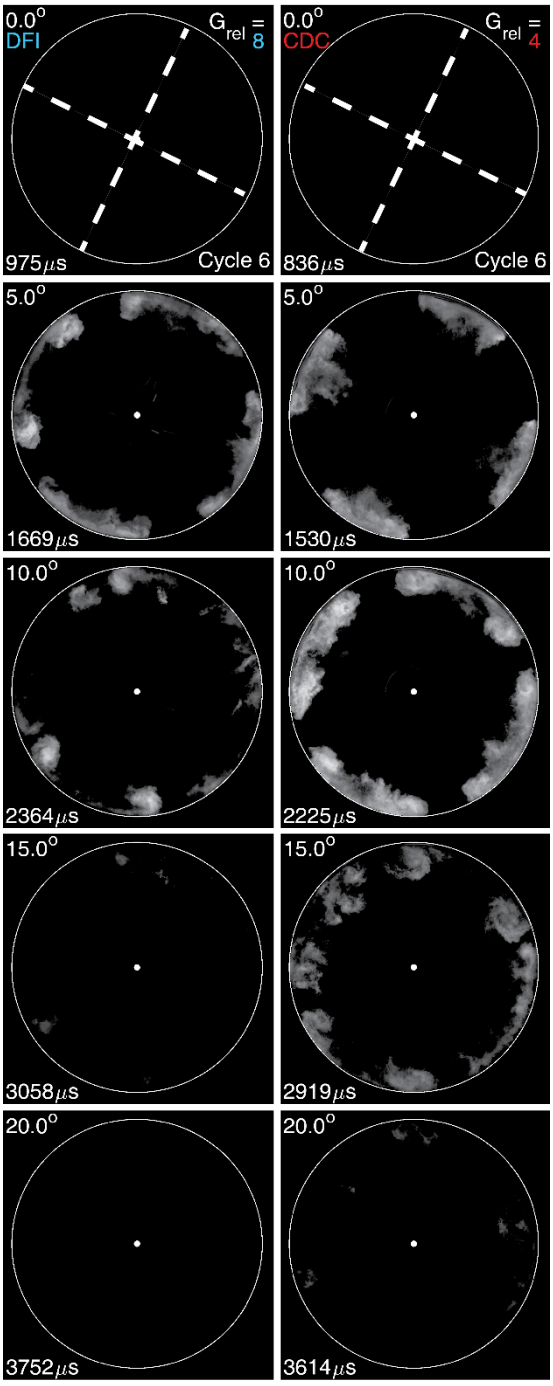

Figure 6. NL images of DFI (left column) vs. CDC (right column) at 0, 5, 10, 15, and 20 CAD ATDC for 18 mol% O_2. The dashed lines in the top row of images represent the axes on which the fuel is injected.

emissions decrease more quickly with decreasing XO_2 for DFI than for CDC. This results in DFI increasing NO_x by more than 20% at 18 mol% O_2 and attenuating NO_x by more than 7% at 14 mol% O_2.

At low loads DFI also has a positive effect on HC emissions. An attenuation between 45% and 51% is observed. Both DFI and CDC exhibit increasing HC emissions with decreasing XO_2

The CO emissions also increase monotonically with decreasing XO_2 for DFI and CDC. Both have very similar CO emissions in this sweep, with results within 10% for all three cases. This instrument is

also more prone to measurement variation than the others used in this study, so these results indicate that the CO emissions are basically the same, as indicated by the error bars on the percent difference plot at both 16 and 18 mol % O_2.

observed for CDC in this study, where the combustion efficiency decreases with decreasing XO_2.

Figure 7 shows the ignition delay, CA50, and end of combustion (EOC) for DFI and CDC. CA50 and EOC are the crank angles at

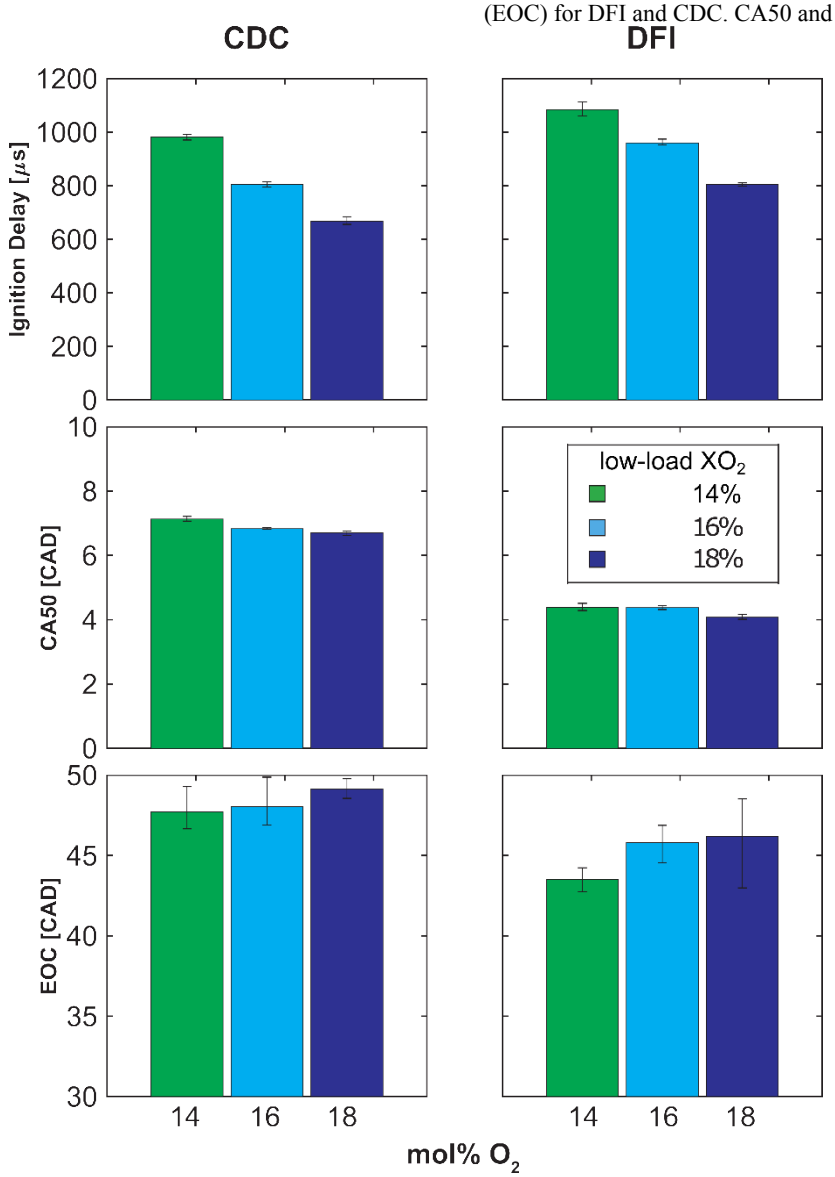

Figure 7. Ignition delay, CA50, and EOC for DFI vs. CDC across the low-load charge-dilution sweep.

Efficiency, load, and combustion phasing

The DOI was held constant in this sweep to keep load approximately constant near 1 bar $IMEP_g$. There was some change in load due to changes in efficiency at different dilution levels, but this variation was less than 0.1 bar $IMEP_g$ between the highest and lowest loads. The maximum load variation between DFI and CDC at the same XO_2 was approximately 6%.

Fuel-conversion efficiency is similar to $IMEP_g$, because it is a function of the work done by the engine divided by the energy in the fuel injected. Due to the low load, the fuel-conversion efficiency is relatively low at approximately 30%. Previous DFI studies have observed that the efficiency of DFI increases as XO_2 decreases [30]. This behavior is also observed in this study. This is unlike what is

which half and 95%, respectively, of the heat release has been completed. This plot shows that the ignition delay for DFI is longer than CDC for each of the points in the sweep, and ignition delay increases with decreased XO_2. The longer ignition delay observed in this study is consistent with previous DFI studies in constant-volume vessels and engines [23,24,27].

CA50 is an important metric when looking at NO_x emissions. It has been shown that advancing CA50 correlates with increasing NO_x emissions, due to longer residence times at higher in-cylinder temperatures [32]. In Figure 5, DFI is shown to have higher NO_x emissions than CDC at two of the three points in the sweep. Figure 7 shows that CA50 is approximately 3 CAD earlier for DFI than for CDC regardless of charge dilution level. The shift in CA50 for DFI could be responsible for the observed increase in NO_x. CA50 is retarded for both CDC and DFI as XO_2 decreases.

EOC is an important metric in this study because of its tie-in with efficiency. The thermal efficiency, η_{th}, of a constant-pressure combustion cycle can be expressed as:

$$\eta_{th} = 1 - \frac{1}{r^{\gamma-1}}\left(\frac{\alpha^{\gamma}-1}{\gamma(\alpha-1)}\right),$$

where α is the cut-off ratio, r is the compression ratio, and γ is the ratio of the specific heats [33]. The cut-off ratio is the ratio of in-cylinder volumes at the end vs. the start of the constant pressure cycle. The constant pressure cycle is a basic approximation of a diesel cycle. The smaller α is, the higher the thermal efficiency. A smaller α results from short heat-release duration. DFI has a heat-release duration that ends approximately 3 CAD earlier than CDC, suggesting DFI should have a higher thermal efficiency, everything else being equal. This is not what was observed in this study; hence, the loss of efficiency for DFI is tied to something other than the combustion duration.

In Figure 6, the NL in the images is concentrated more closely to the piston bowl-rim for DFI than CDC. The closer location of the hot soot to the bowl-rim suggests that DFI may lose more heat to the piston due to closer proximity of the high temperature regions. The same points where efficiency is decreased the most by DFI are also the points where NO_x emissions are increased the most. The increase in NO_x emissions suggests higher combustion temperatures, probably due to earlier CA50 timing. Higher heat losses due to higher combustion temperatures in conjunction with the combustion being closer to the wall may explain the decreased η_f for DFI.

At low-load conditions, the coefficient of variation (COV) of $IMEP_g$ can be a concern, because large COVs can result in an unsteady idle. In this study, the COV of $IMEP_g$ was similar for DFI and CDC at approximately 2.3%.

Higher-Load Condition

This condition was tested to demonstrate how DFI functions when pushed to longer injections and higher injection pressures to reach higher loads. It is important to understand how DFI works at both load limits, because it needs to function well across the entire load range to be a feasible technology for production engines. Due to the small orifice size of the injector used in this study, a relatively long injection duration and high injection pressure had to be used to achieve the higher-load condition.

Soot attenuation

Figure 8 shows the emissions and efficiency results for DFI and CDC at the higher-load condition. The percent difference shown in the bottom half of the figure is calculated the same way as in the low-load sweep discussed previously. This figure shows that DFI attenuates soot at this condition by 27% while decreasing ΣSINL by 73%. This attenuation of soot is significant but less than has been observed in previous DFI studies. This difference in attenuation of soot by DFI is due to an increase in soot emissions with load for DFI and a decrease for CDC. Nevertheless, it should be noted that the engine-out soot at this condition is less than one-quarter of the

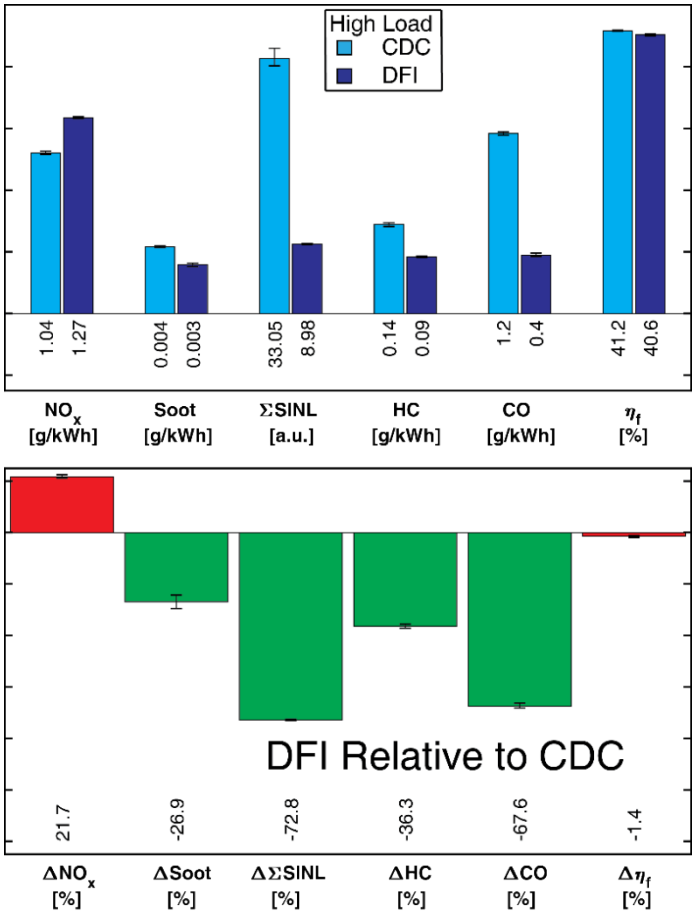

Figure 8. NO_x, soot, ΣSINL, HC, CO, and η_f for CDC and DFI (upper plot), and the percent change for DFI relative to CDC (bottom plot) for the higher-load condition.

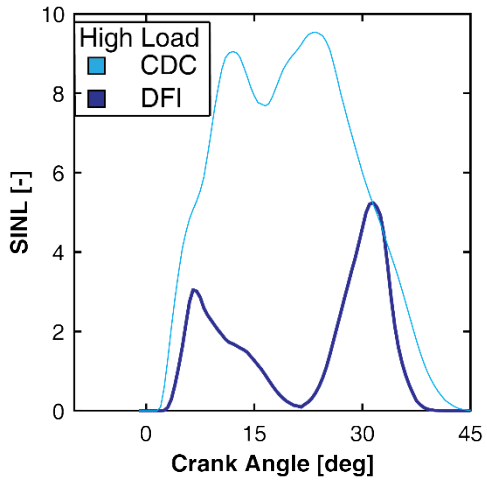

Figure 9. SINL for DFI vs. CDC at the higher-load condition.

regulated limit of 0.013 g/kWh for heavy-duty on-highway trucks in the United States [34].

Figure 9 shows the SINL curves for DFI and CDC. This figure shows that DFI has a lower SINL than CDC for almost the entire duration of the combustion event. The figure also shows that DFI has a second spike in SINL at about 30 CAD. CDC has a second peak in a similar location but the dip in the SINL curve for CDC before the second peak is much smaller. This spike has been observed in a previous study, and it correlates with increased engine-out soot for DFI [30]. The increase in engine-out soot is likely due to the soot being created late in the cycle when temperatures are lower and there is less time available for oxidizing the soot after it is created. The second spike in SINL may be due to interaction between neighboring sprays and/or entrainment of combustion products upstream of the lift-off length [15]. Previous work has shown that the second spike correlates with increased injection pressure and longer injection duration [30]. This higher-load condition has both long injection duration and high injection pressure. When a more-realistic orifice size is used, a lower injection pressure and shorter duration will be used, which is expected to mitigate this issue somewhat.

Engine-out NO_x, HC, and CO emissions

Figure 8 shows that DFI again increases NO_x emissions at the high-load conditions. This behavior has been observed in previous studies as well as in the low-load charge-dilution sweep of the current study. This may be due to DFI advancing CA50. Figure 10 shows that DFI has a CA50 approximately 3 CAD earlier than CDC. This could explain part of the increase in NO_x emissions. DFI can enable improved NO_x emissions by allowing the use of lower XO_2 while keeping soot emissions at acceptable levels. At this condition, the soot levels are quite low, so using DFI is not as advantageous as in the low-load sweep discussed earlier in this study.

At this condition, DFI attenuates HC emissions by 36% and attenuates CO emissions by 68%. This decrease in emissions results in a higher combustion efficiency for DFI. These decreases in emissions are substantial and are similar to the decreases in HC and CO that have been observed at other conditions in previous studies.

Load, efficiency, and combustion phasing

Load for the engine in the study is approximately 10 bar $IMEP_g$. This is the highest load that has been reported with DFI to this point.

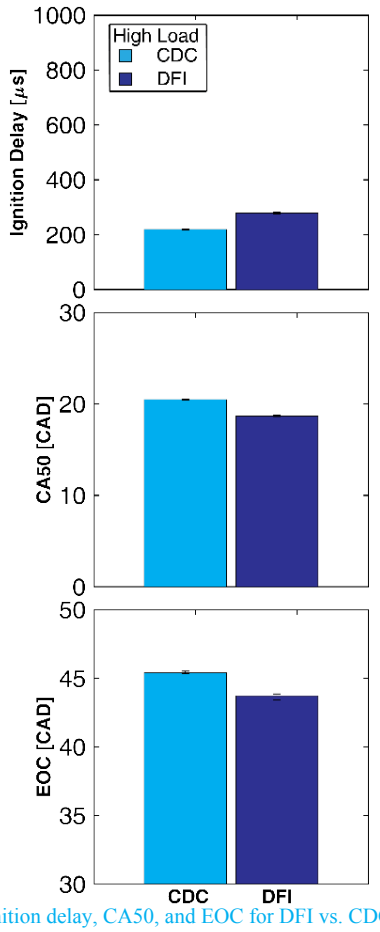

Figure 10. Ignition delay, CA50, and EOC for DFI vs. CDC at the higher-load condition.

Achieving 10 bar $IMEP_g$ is an important threshold, because the ability of DFI to achieve practical loads has not been confirmed. Nevertheless, this is still significantly below the maximum $IMEP_g$ in production heavy-duty diesel engines.

The fuel-conversion efficiency of DFI is lower at this condition, as it has been at most of the other conditions tested. Here it is decreased by 1.4% (relative, not absolute). The analysis done earlier in this study suggests that this may be due to increased heat loss through the piston and cylinder walls. Exhaust temperature is approximately 1 °C lower for DFI than CDC. This supports the argument that DFI loses more heat into the piston or cylinder walls.

Figure 10 shows that the ignition delay is shorter for CDC than for DFI by about 50 µs (< 0.5 CAD). EOC is approximately 2 CAD earlier for DFI than for CDC at this condition. As was the case for the low-load condition, this suggests that the fuel-conversion efficiency loss with DFI is due to factor(s) other than longer combustion duration.

Summary

This paper presents the results from an experimental study using ducted fuel injection (DFI) to attenuate soot formation in a mixing-controlled compression-ignition engine and comparing the results to conventional diesel combustion (CDC). This paper presents both lower-and higher-load results than have been documented previously with DFI in an engine. The lower-load results presented in this study

are of particular relevance because of pending future regulations on idle emissions.

The low-load sweep portion of this study shows that DFI can break the soot-NO_x tradeoff with XO_2. The soot attenuation of DFI relative to CDC is more than 90% across the sweep. The smoke meter is below its sensitivity limit for the entire DFI portion of the sweep. At the lowest XO_2 tested, 14 mol% O_2, DFI attenuates NO_x, soot, and HC emissions relative to CDC. The 14 mol% O_2 DFI condition attenuates NO_x by nearly 90% and soot by over 80% relative to CDC at the 18 mol% O_2 condition. DFI also achieves its highest efficiency at this condition, where it has an efficiency penalty of only 0.6% (relative, not absolute). This sweep shows that DFI enables operation at low-load conditions with significantly lower NO_x and soot emissions.

The higher-load condition is also important because DFI needs to work across the entire load range to be an effective technology. Intermediate-load conditions have been tested in previous studies and shown to be effective. The load range was extended by increasing injection pressure and injection duration while using small injector orifices. This results in a smaller-than-expected soot attenuation with DFI. Despite not being as effective at soot attenuation as previously observed, DFI remains beneficial at this operating point, and the soot emissions are easily compliant with current emissions regulations for on-highway truck engines. Using larger injector orifices and correspondingly shorter injection duration and/or lower injection pressure to achieve high load may be more beneficial, but this approach is yet to be explored.

DFI research is still in its early stages. More work is needed to understand how DFI works, how to calibrate it effectively, and what its limitations might be. More will need to be done to improve the performance of DFI by optimizing duct geometry and operating conditions. With further work on optimizing design and calibration parameters, even better results should be achievable with DFI.

Conclusions

Based on the conducted work and preceding discussion, the following conclusions can be drawn:

- DFI is effective at attenuating engine-out soot emissions across a load range from 1 to 10 bar $IMEP_g$.
- DFI has been observed to break the soot/NO_x trade-off with charge dilution at low-load conditions.
- DFI allows for both low soot and NO_x levels that are not achievable with CDC at low-load conditions.
- DFI significantly lowers HC emissions at all points in this study.
- DFI may require a different calibration than CDC to achieve optimal results.

References

1. Ramanathan, V. and Carmichael, G., "Global and Regional Climate Changes Due to Black Carbon," *Nat Geosci* 1(4):221-227, 2008.

2. Johnson, T. and Joshi, A., "Review of Vehicle Engine Efficiency and Emissions," SAE Technical Paper 2017-01-0907, 2017, doi:https://doi.org/10.4271/2017-01-0907.

3. Johnson, T., "Vehicular Emissions in Review," SAE Technical Paper 2016-01-0919, 2016, doi:https://doi.org/10.4271/2016-01-0919.

4. Maik, B., Kirchner, U., Vogt, R., and Benter, T., "On-Road and Laboratory Investigation of Low-Level PM Emissions of a Modern Diesel Particulate Filter Equipped Diesel Passenger Car," *Atmos Environ* 43(11):1908-1916, 2009.

5. Twigg, M.V., "Progress and Future Challenges in Controlling Automotive Exhaust Gas Emissions," *Appl Catal B-Environ* 70(1-4):2-15, 2007.

6. Wissink, M. and Reitz, R.D., "Direct Dual Fuel Stratification, a Path to Combine the Benefits of RCCI and PPC," *SAE Int. J. Engines* 8(2):878-889, 2015, doi:10.4271/2015-01-0856.

7. Reitz, R.D. and Duraisamy, G., "Review of High Efficiency and Clean Reactivity Controlled Compression Ignition (RCCI) Combustion in Internal Combustion Engines," *Prog Energy Combust Sci* 46:12-71, 2015.

8. Dec, J.E., Yang, Y., Dernotte, J., and Ji, C., "Effects of Gasoline Reactivity and Ethanol Content on Boosted, Premixed and Partially Stratified Low-Temperature Gasoline Combustion (LTGC)," SAE Technical Paper 2015-01-0813, *SAE Int. J. Engines* 8(3):935-955, 2015, doi:10.4271/2015-01-0813.

9. Dempsey, A.B., Walker, N.R., Gingrich, E., and Reitz, R.D., "Comparison of Low Temperature Combustion Strategies for Advanced Compression Ignition Engines with a Focus on Controllability," *Combust Sci Technol* 186(2):210-241, 2014.

10. Saxena, S. and Bedoya, I.D., "Fundamental Phenomena Affecting Low Temperature Combustion and HCCI Engines, High Load Limits and Strategies for Extending These Limits," *Prog Energy Combust Sci* 39(5):457-488, 2013.

11. Musculus, M.P.B., Miles, P.C., and Pickett, L.M., "Conceptual Models for Partially Premixed Low-Temperature Diesel Combustion," *Prog Energy Combust Sci* 39(2-3):246-283, 2013.

12. Splitter, D., Wissink, M., DelVescovo, D., and Reitz, R.D., "RCCI Engine Operation Towards 60% Thermal Efficiency," SAE Technical Paper 2013-01-0279, 2013, doi: 10.4271/2013-01-0279.

13. Naseri, M., Chatterjee, S., Castagnola, M., Chen, H.-Y., et al., "Development of Scr on Diesel Particulate Filter System for Heavy Duty Applications," SAE Technical Paper 2011-01-1312, *SAE Int. J. Engines* 4(1):1798-1809, 2011, doi:https://doi.org/10.4271/2011-01-1312.

14. Pickett, L.M. and Siebers, D.L., "Non-Sooting, Low Flame Temperature Mixing-Controlled DI Diesel Combustion," *SAE Trans* 113(4):614-630, 2004.

15. Polonowski, C.J., Mueller, C.J., Gehrke, C.R., Bazyn, T., et al., "An Experimental Investigation of Low-Soot and Soot-Free Combustion Strategies in a Heavy-Duty, Single-Cylinder, Direct-Injection, Optical Diesel Engine," *SAE*

International Journal of Fuels and Lubricants 5(1):51-77, 2011.
16. Manin, J., Skeen, S., Pickett, L., Kurtz, E., et al., "Effects of Oxygenated Fuels on Combustion and Soot Formation/Oxidation Processes," *SAE Int. J. Fuels Lubr.* 7(3):704-717, 2014, doi:10.4271/2014-01-2657.
17. Higgins, B. and Siebers, D.L., "Measurement of the Flame Lift-Off Location on D.I. Diesel Sprays Using OH Chemiluminescence," *SAE Trans* 110(3):739-753, 2001, doi:10.4271/2001-01-0918.
18. Pickett, L.M. and Siebers, D.L., "Soot Formation in Diesel Fuel Jets near the Lift-Off Length," *International Journal of Engine Research* 7(2):103-130, 2006.
19. Gehmlich, R.K., Dumitrescu, C.E., Wang, Y., and Mueller, C.J., "Leaner Lifted-Flame Combustion Enabled by the Use of an Oxygenated Fuel in an Optical CI Engine," 2016, doi:https://doi.org/10.4271/2016-01-0730.
20. Ou, L., Cai, H., Seong, H.J., Longman, D.E., et al., "Co-Optimization of Heavy-Duty Fuels and Engines: Cost Benefit Analysis and Implications," *Environmental Science & Technology* 53(21):12904-12913, 2019.
21. "Global EV Outlook 2019," International Energy Agency, Online source, https://webstore.iea.org/global-ev-outlook-2019.
22. Bunsen, R. and Roscoe, H.E., "Photo-Chemical Researches. Part I. Measurement of the Chemical Action of Light," *Philosophical Transactions of the Royal Society of London* 147:355-380, 1857.
23. Mueller, C.J., Nilsen, C.W., Ruth, D.J., Gehmlich, R.K., et al., "Ducted Fuel Injection: A New Approach for Lowering Soot Emissions from Direct-Injection Engines," *Appl Energ* 204:206-220, 2017.
24. Gehmlich, R.K., Mueller, C.J., Ruth, D.J., Nilsen, C.W., et al., "Using Ducted Fuel Injection to Attenuate or Prevent Soot Formation in Mixing Controlled Combustion Strategies for Engine Applications," *Appl Energ* 226:1169-1186, 2018.
25. Fitzgerald, R.P., Svensson, K., Martin, G., Qi, Y., et al., "Early Investigation of Ducted Fuel Injection for Reducing Soot in Mixing-Controlled Diesel Flames," SAE Technical Paper 2018-01-0238, 2018, doi:https://doi.org/10.4271/2018-01-0238.
26. Svensson, K.I. and Martin, G.C., "Ducted Fuel Injection: Effects of Stand-Off Distance and Duct Length on Soot Reduction," SAE Technical Paper 2019-01-0545, 2019, doi:https://doi.org/10.4271/2019-01-0545.
27. Nilsen, C.W., Biles, D.E., and Mueller, C.J., "Using Ducted Fuel Injection to Attenuate Soot Formation in a Mixing-Controlled Compression Ignition Engine," SAE Technical Paper 03-12-03-0021, *SAE Int. J. Engines* 12(3):309-322, 2019, doi:https://doi.org/10.4271/03-12-03-0021.
28. Tanno, S., Kawakami, J., Kitano, K., and Hashizume, T., "Investigation of a Novel Leaner Fuel Spray Formation for Reducing Soot in Diffusive Diesel Combustion - Homogenizing Equivlence Ratio Distribution in the Lift-Off Region-," SAE Technical Paper 2019-01-2273, *SAE Int.*, 2019.
29. Li, F., Lee, C.-f., Wu, H., Wang, Z., et al., "An Optical Investigation on Spray Macroscopic Characteristics of Ducted Fuel Injection," *Exp Therm Fluid Sci* Volume 109, 2019.
30. Nilsen, C.W., Biles, D.E., Yraguen, B.F., and Mueller, C.J., "Ducted Fuel Injection Vs. Conventional Diesel Combustion: An Operating-Parameter Sensitivity Study Conducted in an Optical Engine with a Four-Orifice Fuel Injector," SAE Technical Paper 03-13-03-0023, *SAE Int. J. Engines*, 2020.
31. Mueller, C.J. and Martin, G.C., "Effects of Oxygenated Compounds on Combustion and Soot Evolution in a DI Diesel Engine: Broadband Natural Luminosity Imaging," *SAE Trans* 111(4):518-537, 2002, doi:10.4271/2002-01-1631.
32. Valentino, G., Iannuzzi, S., and Corcione, F.E., "Experimental Investigation on the Combustion and Emissions of a Light Duty Diesel Engine Fuelled with Butanol-Diesel Blend," SAE Technical Paper 2013-01-0915, 2013, doi:https://doi.org/10.4271/2013-01-0915.
33. Heywood, J.B., Internal Combustion Engine Fundamentals. McGraw-Hill, New York, 1988.
34. "Heavy-Duty Highway Compression-Ignition Engines and Urban Buses: Exhaust Emission Standards," 2016.

Contact Information

Acknowledgments

This research was conducted as part of the Advanced Combustion Engines program sponsored by the U.S. Department of Energy, Office of Energy Efficiency and Renewable Energy, Vehicle Technologies Office. The authors gratefully acknowledge Vehicle Technologies Office Program Managers Gurpreet Singh, Michael Weismiller, and Kevin Stork for long-term support of the research programs of which this study is a component. The authors also would like to thank Prof. Jean-Pierre Delplanque, Christopher Nilsen's advisor at the University of California, Davis, for his assistance and feedback on this project. The research was conducted at the Combustion Research Facility, Sandia National Laboratories, Livermore, California. Sandia National Laboratories is a multi-mission laboratory managed and operated by National Technology and Engineering Solutions of Sandia, LLC, a wholly owned subsidiary of Honeywell International, Inc., for the U.S. Department of Energy's National Nuclear Security Administration under contract DE-NA-0003525. This paper describes objective technical results and analysis. Any subjective views or opinions that might be expressed in the paper do not necessarily represent the views of the U.S. Department of Energy or the United States Government.

Definitions/Abbreviations

AHRR	apparent heat release rate
BMEP	brake mean effective pressure
CA50	crank angle where 50% of energy has been released
CAD	crank angle degree
CDC	conventional diesel combustion

CF_B	No. 2 diesel emissions certification fuel containing < 15 parts per million sulfur
CO	carbon monoxide
CO_2	carbon dioxide
DFI	ducted fuel injection
DOI	duration of injection
charge dilution	simulated exhaust gas recirculation, achieved by adding nitrogen gas to the intake air
EI	emissions index
EOC	end of combustion
HC	hydrocarbons
HCCI	homogeneous-charge compression-ignition
ICE	internal combustion engine
IMAP	intake manifold absolute pressure
$IMEP_g$	gross indicated mean effective pressure
IS	indicated specific
LLFC	leaner-lifted-flame-combustion
LTGC	low-temperature gasoline combustion
MCCI	mixing-controlled compression-ignition
n_{comp}	polytropic compression coefficent
NL	natural luminosity
NO_x	nitrogen oxides
O_2	oxygen
PM	particulate matter
RPM	revolutions per minute
SINL	spatially integrated natural luminosity
SOC	start of combustion
TDC	top dead center
XO_2	O_2 molar fraction
η_f	fuel-conversion efficiency
η_{th}	thermal efficiency